Journal of the European Ceramic Society 20 (2000) 1493–1503

TEM study of carbon fibre reinforced aluminium matrix composites: influence of brittle phases and interface on mechanical properties

M. Lancin *, C. Marhic

Physique Cristalline, Institut des Matériaux Jean Rouxel, BP 32 229 Nantes cedex 3, France

Received 13 May 1999; received in revised form 4 November 1999; accepted 8 November 2000

Abstract

The microstructure of A357 aluminium alloy (7 wt% Si + 0.6 wt% Mg) reinforced by 1D-M40J carbon fibres is characterised using different techniques of transmission electron microscopy (diffraction, HRTEM, EDX, EELS). The microstructure of the high modulus PAN based fibre and of the pyrolytic carbon coating (Cp) is fully characterised. Silicon and Mg_2Si grains which determine matrix-reinforcement adhesion are investigated. On the basis of the microstructural features, the mechanical properties of the composites are discussed. The mechanical behaviour of composites prepared with and without Cp interphases corresponds to a brittle matrix reinforced by brittle fibres. In the case of the composite without Cp interphase, the most influent parameter is the high resistance to sliding at the interface between silicon and fibres which leads to a strong fibre-matrix "bonding" and thus, to a weak and brittle material. The interfacial resistance to decohesion and to sliding is lower in the composite with Cp interphase resulting in higher strength and limited pull out. This lower interfacial resistance is due to the successive microporous and layered microstructures of the pyrolytic carbon coating.

Keywords: Al alloy; Al_4C_3; Carbon fibre; Composites; Electron microscopy; Interphase; Mechanical properties

1. Introduction

Carbon fibres are used to increase strength and stiffness of aluminium alloys while keeping low weight and good thermal and electrical conductivity. However, brittle phases which form or precipitate during the processing may have a deleterious influence on the mechanical properties of the composites.[1–11] Studies are being performed to improve the processing and to obtain the required properties. C/Al composites prepared at ONERA-Chatillon for aerospace applications contain a high volume fraction of fibres (70%).[12,13] In one of these, an A357 aluminium alloy is reinforced with high modulus M40J carbon fibres, sometimes coated with a pyrolytic carbon interphase (Cp). The M40J/A357 composite without the Cp interphase is brittle and weak (≈700 MPa).[13] The M40J/Cp/A357 composite with the Cp interphase is stronger (≈1360 MPa) but less so than expected from the law of mixtures and, moreover, it is rather brittle (limited pseudo-plastic deformation, low work of fracture), despite some fibre debonding.[14] Scanning electron microscopy (SEM) did not reveal any reaction layer in either type of composite.[13] A transmission electron microscopy (TEM) study was thus performed to reach a full knowledge of the microstructural features of the materials and a better understanding of their mechanical behaviour. The mechanical tests and properties are fully described in a paper previously published.[14]

In this paper, the microstucture of the high modulus carbon fibre and of the carbon coating is characterised. The amounts and locations of the brittle phases, aluminium carbides and silicon, are determined. Interdiffusion, which is known to influence the failure resistance at the interfaces, is also studied. The discussion of the microstructural features reveals important parameters and shows that the mechanical behaviour of the composites does not depend on the metal matrix. Models developed for ceramic–ceramic composites are successfully used to analyse the mechanical properties.

2. Materials and experimental procedure

1D-composites were fabricated with A357 alloy (alloying elements: Si = 7 wt%, Mg = 0.6 wt%) and M40J fibres (σ_r = 4400 MPa, E = 377 GPa)- by liquid metal infiltration (LMI), under moderate pressure

* Corresponding author now at: TECSEN Laboratory, case 231, 13397 Marseille Cedex 20, France.
E-mail address: lancin@matop.u-3mrs.fr (M. Lancin).

0955-2219/00/$ - see front matter
PII: S0955-2219(00)00021-2

(15 MPa), during 1 min, at 918 K.[13] Two composites were obtained using respectively bare fibres or fibres coated by pyrolytic carbon (Cp), both containing a high volume fraction of fibres (≈70%).

Longitudinal and cross sections were prepared by mechanical grinding and ion thinning. During grinding and polishing, the cohesion of the samples was maintained by using an appropriate glue and a Ti ring (Balzers). These necessary precautions and the occurrence of cracks sometimes observed between fibres and matrix (Fig. 1a) reveal the weak adhesion between fibres and matrix in both composites. Ion thinning is carried out in a Balzers ion thinner using a low beam density and a sample holder cooled with liquid nitrogen. The composite microstructure is not modified by such ion thinning conditions.

Phase identification and localisation were performed by electron diffraction patterns (EDP) and nanodiffraction, high resolution transmission electron microscopy (HRTEM), energy dispersive X-rays spectroscopy (EDX) and electron energy loss spectroscopy (EELS). Experiments were carried out using a field emission gun (FEG) HF2000 Hitachi microscope (200 KV, Scherzer resolution = 2.6 Å) equipped with a CCD camera (MSC Gatan), a Si-Li detector (Kevex Super Quantek) and a PEELS (Gatan). Analyses were performed using a cooling holder (Gatan), a 4–10 nm probe size and a 12° tilt angle for EDX spectroscopy.

3. Results

Many microstructural features are shared by the two composites. We thus describe them and underline the differences where they occur.

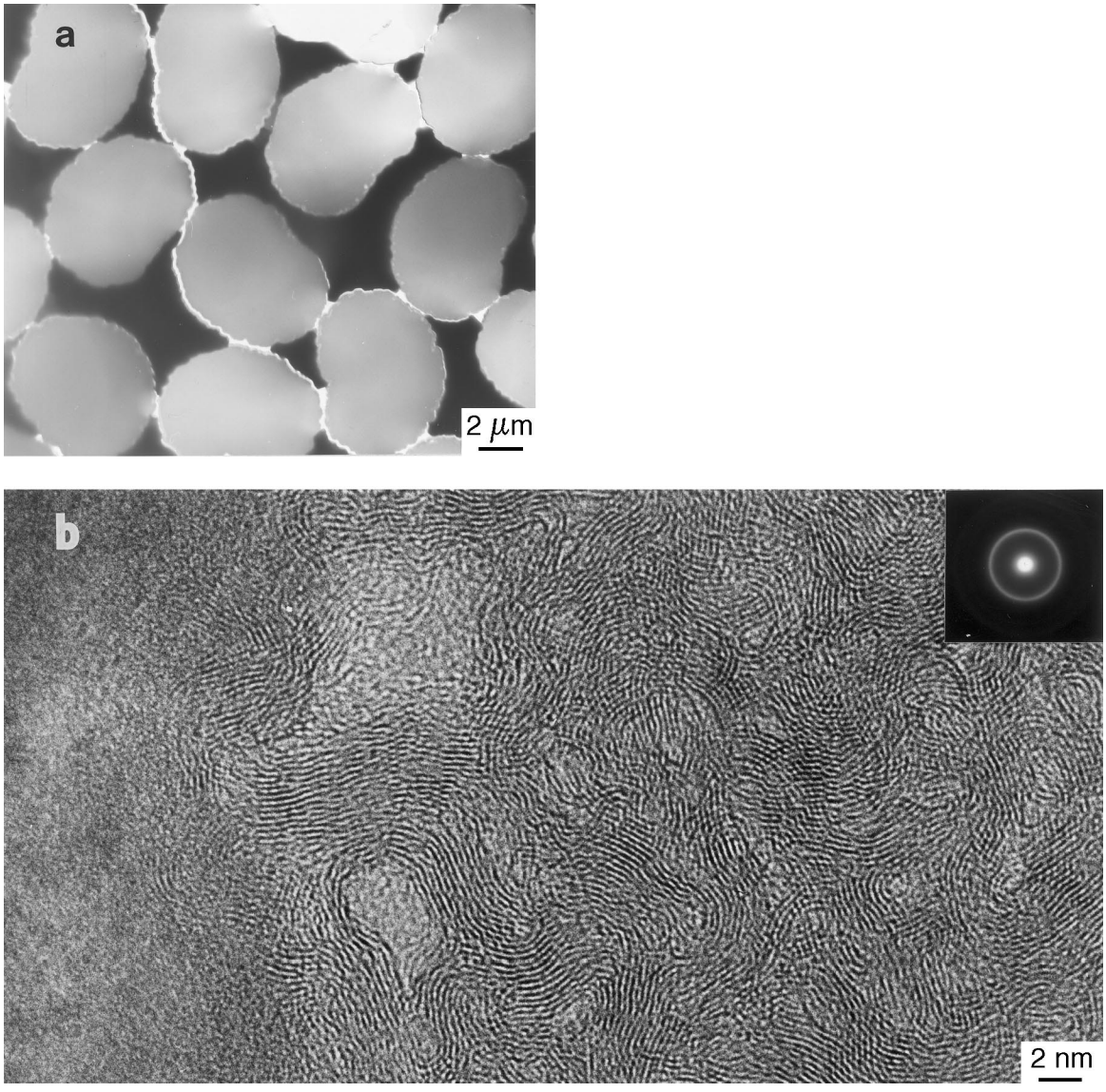

Fig. 1. Microstructure of a cross-section of the M40J/A357 composite. Bright field (a) and HRTEM (b) images of the Al/fibre interface. (b) Shows the folded aromatic layers surrounding porosities and the EDP characteristic of equiaxed {0002} carbon planes.

3.1. Reinforcement

The mechanical properties of the composites depend on the microstructure of the reinforcement after the processing. The microstructural features of the fibre and of the Cp were thus investigated on longitudinal and cross-sections of the M40J/A357 and M40J/Cp/A357 composites respectively.

3.1.1. Microstructure of M40J carbon fibre

The fibres are regularly distributed in the composites. Their bean shaped cross-section (Fig. 1a) is fringed with roughness ranging from a few nanometers to a few microns in size (Figs. 1, 4a, 5, 6, 7, 8). Their longitudinal section is more regular than their cross-section but the surface is wavy, with an amplitude which reaches 10 nanometers or so (Fig. 2a). Owing to their bean-shaped

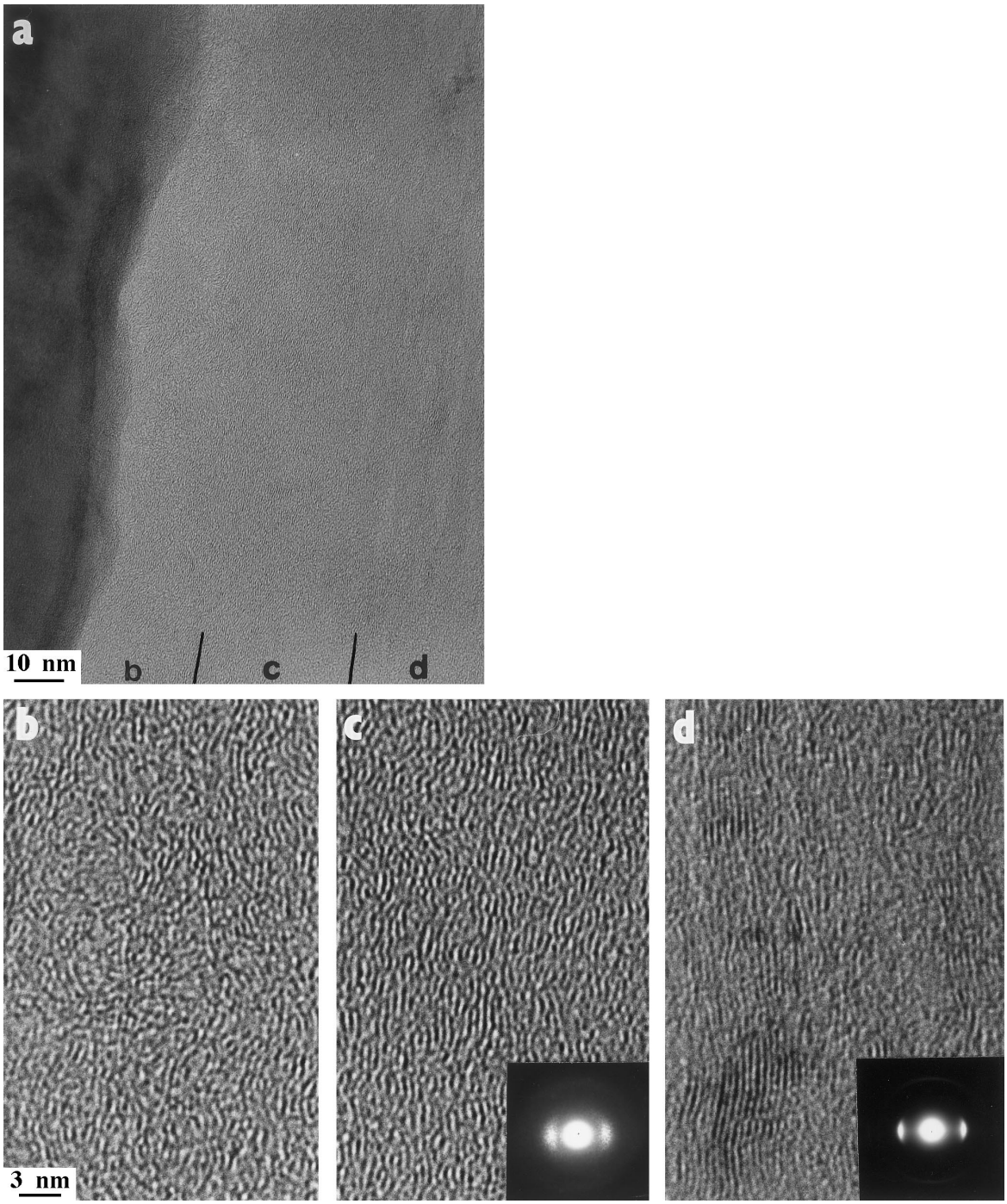

Fig. 2. Microstructure of a longitudinal section of the M40J/Cp/A357 composite. Bright field image of the Al/Cp/fibre interface (a) HRTEM image of the microporous Cp (b), HRTEM images and EDPs of the layered Cp (c) the fibre (d).

cross-section, their fluted surface and their dense packing, the fibres are always in contact with two or three neighbours and are bridged to the others by an irregular and narrow matrix. As a result, the matrix is cut into microlingots and a residual porosity is observed where fibres are in contact.

The fibre section exhibits a uniform contrast in bright field mode (Figs. 4a, 6) except in its outermost part where significant porosity is revealed by its light contrast. This porosity, which is not continuously observed all around the fibre, extends over 10–200 nm beneath the surface. The pore size ranges from 4–20 nm.

Using M40J/A357 cross-sections, the fibre microstructure was characterised. The same diffraction pattern is obtained in the fibre core and in the fibre periphery whatever its porosity (Fig. 1b). This continuous ring pattern is characteristic of equiaxed {0002} planes. HRTEM images confirm these results and reveal the grain size (Fig. 1b). Fibre nanocrystals consist of a stack of a few aromatic layers, one or two nanometers in length, named BSU (Basic Structural Unit[15]). BSUs of similar orientation are associated in clusters named LMO (Local Molecular Orientation[15]) whose width and length rarely exceed 10 nanometers. BSUs are joined by disclinations where atoms are linked by twisted or stretched bonds or tetrahedral bonds as typical in carbon fibres.[16] Such an organisation results in many places in a strong curvature of the aromatic layers, in very sharp angles between them and in a residual porosity. The pore size rarely exceeds a few nanometers in the fibre except near the surface as above mentioned. The folded organisation of the aromatic layers is observed throughout the fibre section even in its outermost part.

HRTEM images of longitudinal sections reveal the length of BSUs and LMOs organised in microfibrils[17] along the fibre axis (Fig. 2d). As in the cross-sections, the BSU length is equal to one or two nanometers and the LMO width perpendicular to the fibre axis is about 10 nm. Unlike the cross-sections, microfibrils extend over several tens of nanometers along the fibre axis and the relative disorientation of aromatic layers is less substantial. EDPs show, indeed, that aromatic planes are aligned to within $\pm 17^{\circ}$ of the fibre axis (Fig. 2d). The space between microfibrils reveals the length of the pore structures (about 50 nm). Because of this microstructure, the fibre is categorised into the large family of turbostratic carbons.

Interdiffusion between aluminium and fibre was studied by EDX (Fig. 3). Aluminium is revealed beneath the fibre surface over about five nanometers but analyses may be influenced by the fibre roughness. Traces of aluminium and silicon are also detected in the fibre just beyong this zone (Fig. 3a), particularly in the pores. In aluminium, carbon is not detected without ambiguity either by EDX or by EELS. A layer of 5 nanometers or so in the matrix next to the Al/C interface contains some oxygen (Fig. 3c).

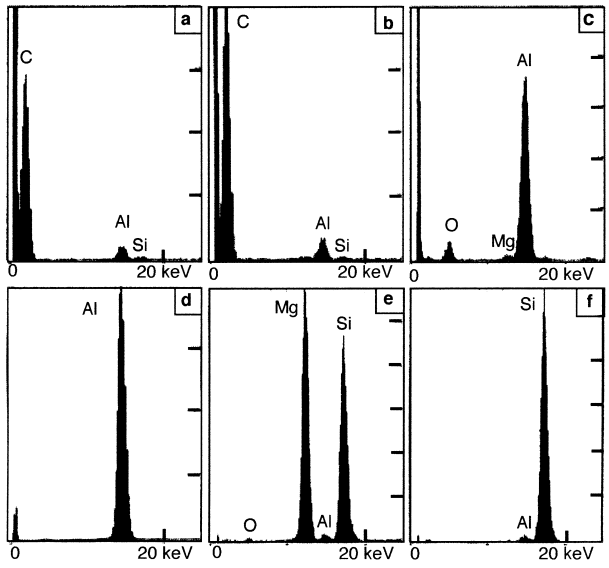

Fig. 3. EDX analysis. Spectra characteristic of the fibre at 20 nm from the interface (a) the microporous Cp (b) Al next to the Al/C interface (c) Al at 20 nm from the Al/C interface (d) Mg_2Si (e) and Si next to the Si/C interface (f).

3.1.2. Microstructure of pyrolytic carbon coating (Cp)

In the M40J/Cp/A357 cross-sections, the Cp coating is identified at the fibre/matrix interface by a light contrast in bright field mode (Figs. 4a, 6b) and by EDPs and HRTEM images (Fig. 4b) which distinguish fibre and Cp. Every fibre is continuously surrounded by the Cp coating, 15–30 nm thick. The Cp, in which aromatic layers are cut into BSUs, exhibits a turbostratic structure. Near the fibres, BSUs tend to form continuous sheets which follow the roughness of the fibre surface and LMOs can hardly be distinguished. The orientation of the aromatic layers varies to within $\pm 35^{\circ}$ with respect to the fibre axis. When the coating thickness exceeds about 10 nanometers, LMOs are more and more distinct and their orientation less and less equiaxed resulting in a microporous microstructure near the matrix.

HRTEM images and EDPs of longitudinal sections confirm the change of the Cp microstructure versus thickness (Fig. 2b,c). Along the fibre surface, over 10 nm or so, we observe a layered structure. As in the cross-sections, LMOs or microfibrils cannot be distinguished on HRTEM micrographs. In the layered zone, the aromatic layers follow the fibre surface and their disorientation versus the fibre ($\pm 25^{\circ}$) is only a little more evident than in the fibre. In the outermost part of the Cp, the microporous microstructure is in excellent agreement with that revealed by HTREM images on cross sections.

In the microporous Cp coating, traces of aluminium, silicon and magnesium are detected by EDX but no other heteroatoms and in particular no oxygen atoms are found (Fig. 3b). In the layered Cp coating, heteroatoms are not detected.

3.2. Brittle phases

Al_4C_3 reaction product and matrix precipitates (Si or Mg_2Si) are identified on cross-sections by electron diffraction, HRTEM, EDX and by plasmon peak energy. Low loss edges permit a more systematic study of the phases than core edges because they are less sensitive to specimen thickness. Moreover, despite the variation of the plasmon peak energy of carbon as a function of the beam orientation versus the basal plane, it was possible to distinguish between the different phases because we found distinct values for the volume plasmon energy

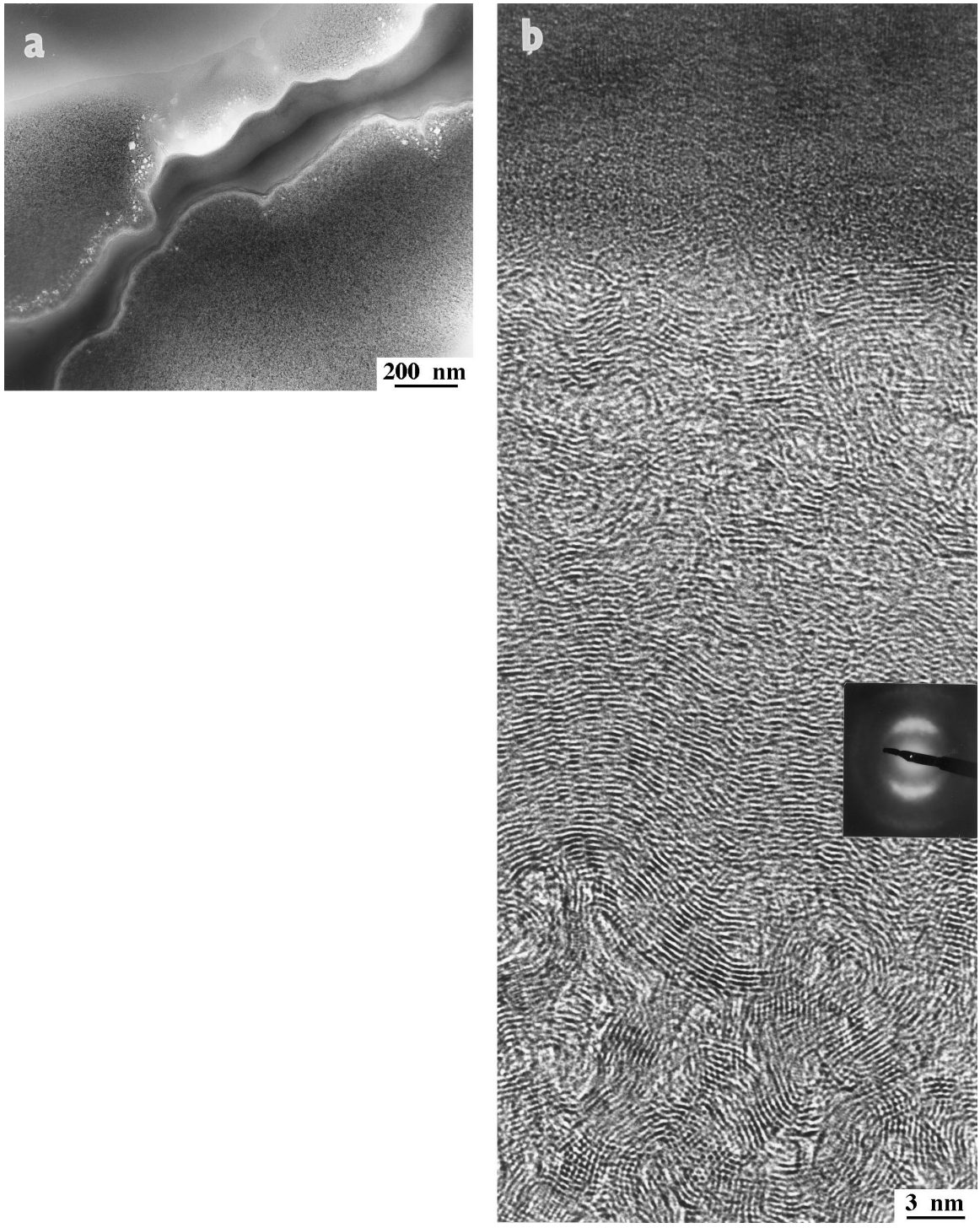

Fig. 4. Microstructure of a cross-section of the M40J/Cp/A357 composite. (a) Bright field image of a fibre/Cp/Al interface where the Cp and the fibre porosities are revealed by a light contrast; (b) HRTEM image showing the layered Cp near the fibre and the microporous Cp near the matrix; EDP of the layered Cp.

(Fig. 6): $E_{Mg2Si} = 12.7$ eV, $E_{Al} = 15$ eV, $E_{Si} = 16.7$ eV, $E_{carbide} = 18.9$ eV and for the different carbons 23.4 eV in microporous Cp, 24.3 eV in layered Cp, 23.7 eV in the fibre and 21 eV in large fibre pores.

3.2.1. Si and Mg_2Si precipitates

The matrix contains Si grains, inhomogeneously distributed in the matrix and located predominantly next to the fibres, generally in contact with two fibres or between them (Fig. 6). All these grains exhibit typical stacking faults; thus their contrast was most often used to identify them. It is noteworthy that the amount of stacking faults is the highest in the narrowest parts of the Si grains which bridge between fibres. The Si grain size generally ranges between a hundred nanometers to about one micron but some nanometric grains are also detected. Si grains contain various amount of inclusions (Fig. 6b,c) in which aluminium is detected but whose exact composition is under study. The largest inclusions were identified as aluminium.

Mg_2Si precipitates a few tens nanometers in size were on occasion identified by EDX in the matrix (Fig. 3e). Mg_2Si precipitates were never detected between the fibres probably because of the low concentration of Mg in the alloy as compared to Si.

3.2.2. Aluminium carbides

In both composites, aluminium carbide grains exhibiting a lath like morphology were revealed at interfaces using the techniques previously mentioned. In contact with the carbon, but not extending into the fibres, the carbide grains are included in the matrix. They are generally located at Al/C interface (Figs. 1b and 7a) but some of them are included in silicon grains (Fig. 7b). The carbide grain length ranges from 100 to 350 nm and their aspect ratio (length/width) from 8 to 15. The amount of carbide grains is difficult to assess because they are irregularly observed at the interfaces. From a systematic study of longitudinal and cross-sections, it is possible to conclude that carbides are rather rare in both composites but rarer at the Cp/matrix interface than at the fibre/matrix interface. Moreover, their amount is clearly lower than that of the Si grains.

3.2.3. Si–C interfaces

HRTEM was performed to study the possible reaction between carbon and silicon resulting in SiC formation

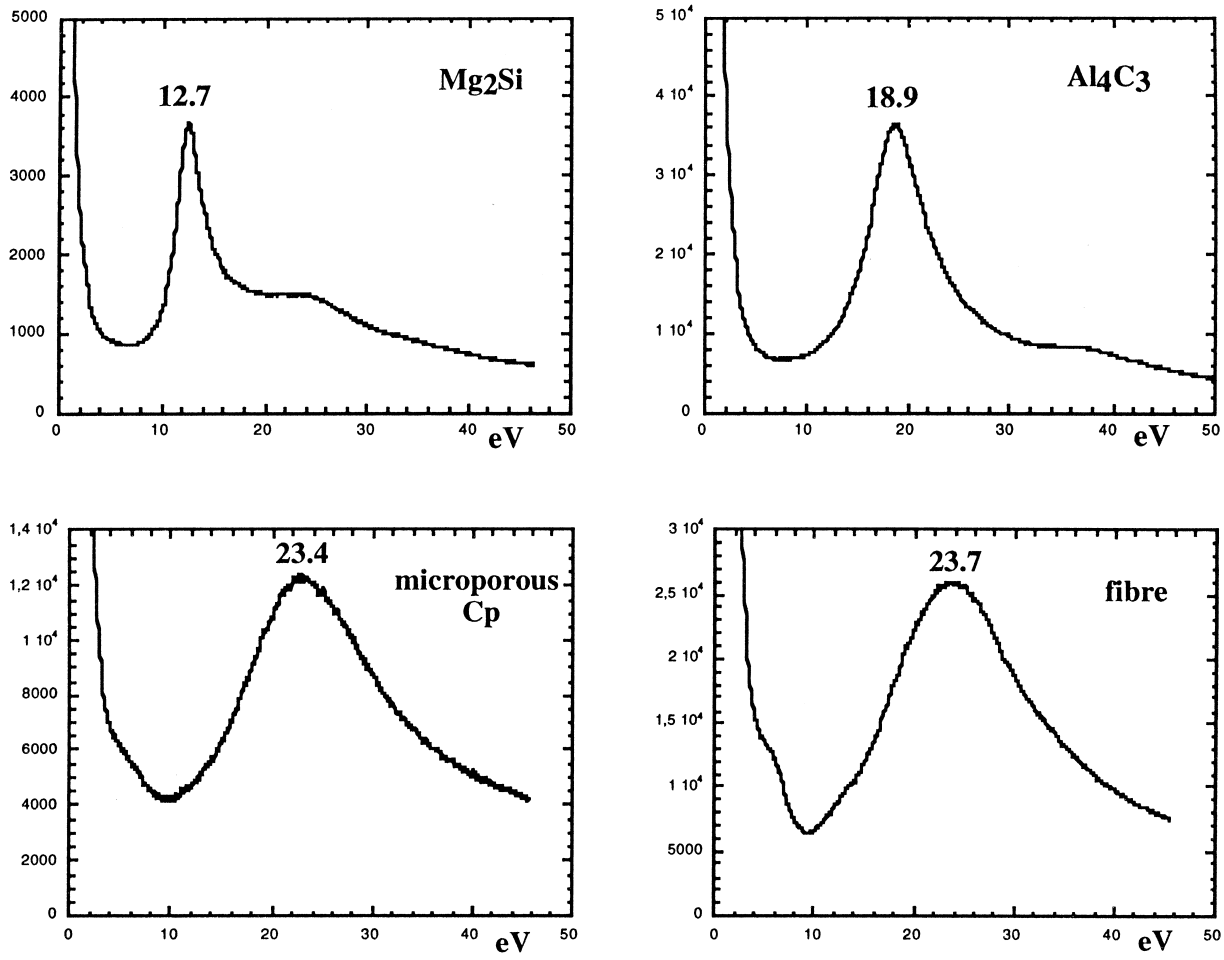

Fig. 5. EELS analysis: volume plasmon peaks.

which has been reported at low temperature (798 K) in Al–Zn alloy.[18] No grains were detected at the Si/C interfaces in either composite (Fig. 8) except for the Al_4C_3 as above mentioned. Thus, the C–Si reaction, if any, is not detectable after liquid metal infiltration.

Interdiffusion is also to a very limited extent detected by EDX in a narrow zone on either side of the interface. Carbon is not detected in the silicon beneath the interface (Fig. 3f) whereas traces of silicon and aluminium are observed in the carbon, the spectrum being similar to that obtained at the Al/C interfaces.

4. Discussion

Brittle phases have been identified at interfaces in both composites. Their influence depends on their brittleness as compared to that of the reinforcement and on the resistance to debonding and to sliding at the interface. Although the Cp coating does not change the strength and the Young modulus of the fibre,[14] it may modify crack propagation in the reinforcement. The resistance to debonding and to sliding between the reinforcement and the different phases, aluminium, aluminium carbide or silicon, will accordingly be analysed using the microstructural features of the interfaces. Finally, we show that the conclusions derived from the microstructural features are consistent with the mechanical behaviour of the composites

4.1. Fibre and Cp microstructure and crack propagation

The turbostratic structure of the M40J fibre is more typical of the high strength PAN-based fibres than of the high modulus ones first described by Guigon et al.[19] The core porosity for example, is close to that observed in ex-Pan high strength T300 fibres by Lamouroux et al.[20] Moreover, in agreement with Feldhoff et al.,[21] we

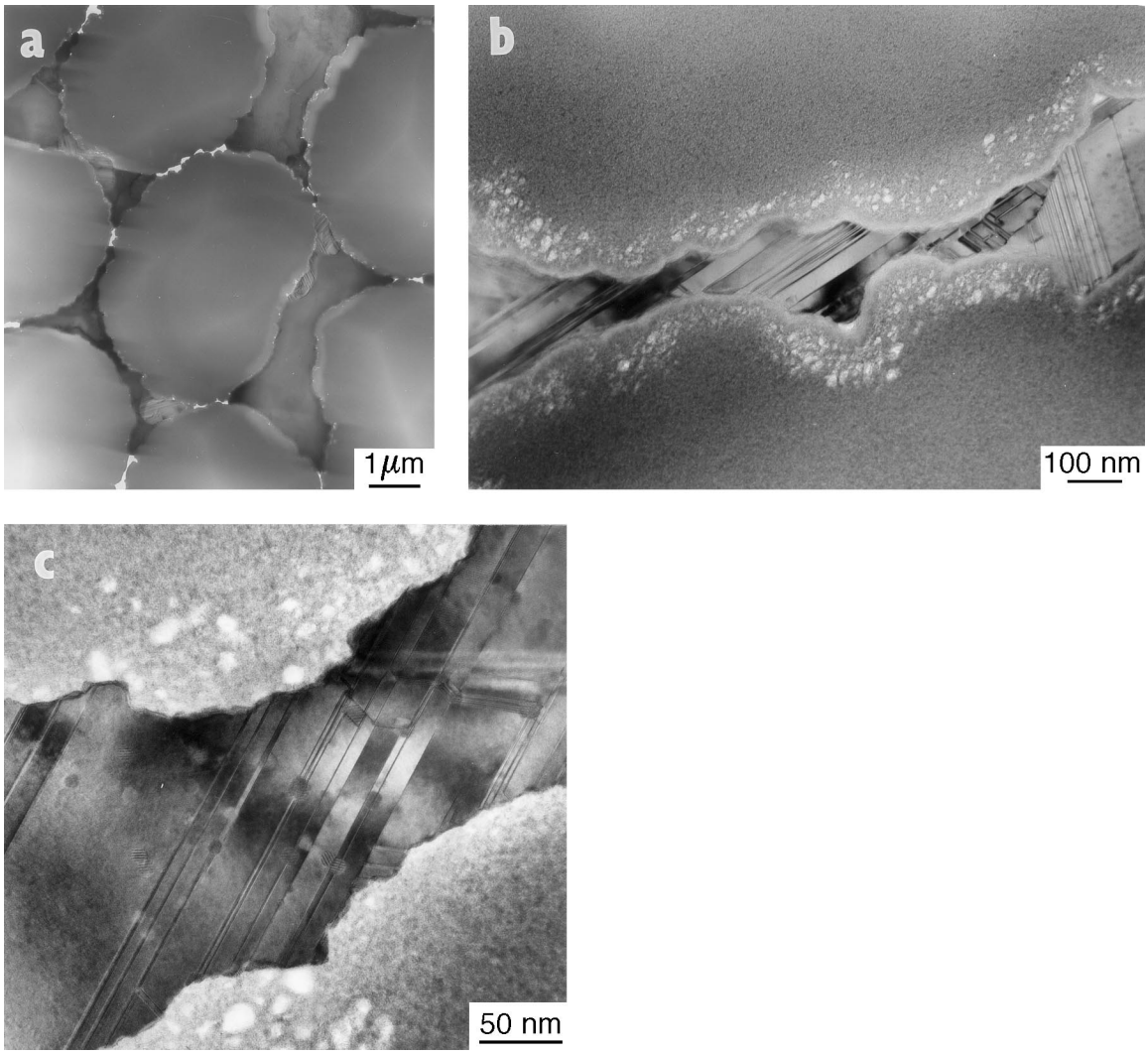

Fig. 6. Silicon grains. Localisation of Si grains in a cross-section thanks to their stacking faults (a). Bright field images of Si grains bridging fibres in M40J/Cp/A357 (b) and in M40J/A357 (c) composites: images reveal stacking faults and Al inclusions in Si and the continuous ribbon of Cp between Si and fibre in (b).

do not observe the layered structure of the outermost part of the fibres mentioned by Guigon et al. in high modulus fibres. The lack of layered structure could be due to some dissolution of the fibre during composite fabrication. However, in any case, the thickness of the possible lamellar layer must be limited in the M40J fibre because the short duration of the LMI and the small amount of aluminium carbide formed are not consistent with extensive dissolution.

Fibre and Cp have different turbostratic structures but both of which could avoid crack propagation through the reinforcement. However, the impact of a possible surface notch is different whether it is applied on the fibre or on the Cp.

The efficiency of pyrolytic carbon as a mechanical fuse is generally ascribed to a layered structure which promotes crack deflection and interface sliding. As for the crack deflection, the complex structure of the Cp is particularly efficient. The outermost part of the Cp exhibits indeed a microporous morphology where the LMOs are equiaxed. Such a structure is very suitable to promote crack branching on the disclinations as well as crack deflection in LMOs in a direction parallel to the {0002} planes and, thus, it is efficient to release stresses at crack tips. If blunted cracks could nevertheless reach the inner part of the Cp, where aromatic layers follow the fibre surface, they could be deflected in a direction parallel to the fibre surface more efficiently than the initial crack. As for the interface sliding, we have to consider the adhesion of the different phases and we discuss the influence of this parameter later.

When submitted to similar stresses than the Cp, the turbostratic structure of the fibre may also promote crack splitting and crack deflection in a direction parallel to its axis because folded aromatic layers are oriented to the fibre axis within $\pm 17^{\circ}$. However, during a tensile

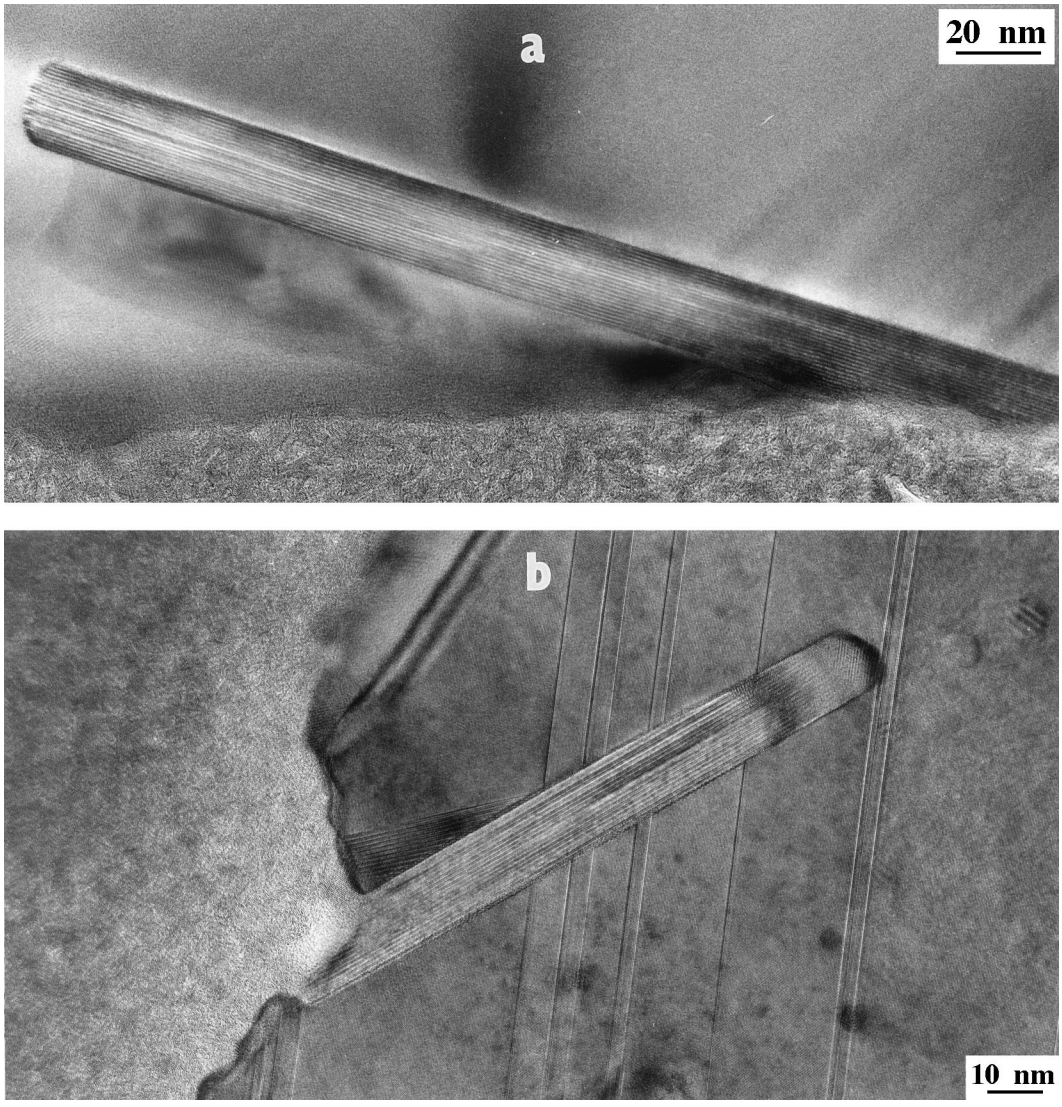

Fig. 7. Identification of Al_4C_3 grains. HRTEM images of Al_4C_3 grains at an Al/fibre interface (a) and included in a silicon grain identified by its characteristic stacking faults and Al inclusions (b). In both Al_4C_3 grains the contrast of {0003} planes is visible.

test, because the fibres are seldom aligned parallel to the applied stress, the notch tip will usually be submitted to shear stresses (failure in mode III[22]) which will promote propagation through the fibre and thus fibre failure.

4.2. Adhesion

Adhesion of aluminium matrix to fibres (bare or coated) is determined by conflicting effects. During LMI, carbon is dissolved in liquid aluminium and aluminium diffuses into the carbon. After quenching, carbon atoms remain in the matrix, even if they are undetectable by TEM, and Al is still observed in the carbon. Therefore, chemical diffusion bonds which are said to be "good" bonds[4] can be considered to link aluminium to fibres. However, we have seen that the matrix is cut into micro-lingots by fibres in contact. During cooling, the shrinkage is determined by the fibres. The coefficient of thermal expansion of aluminium ($23\ 10^{-6}\ K^{-1}$) being higher than the axial ($\simeq -1\ 10^{-6}\ K^{-1}$) and transverse ($\approx -10\ 10^{-6}\ K^{-1}$) coefficients of thermal expansion of a fibre, Al/C interfaces are submitted to radial tension and transverse shear stress which counterbalance the chemical diffusion bond. The aluminium matrix is, however, fixed here and there to the fibres by aluminium carbide grains.

Aluminium carbide grains that are formed by reaction between liquid aluminium and carbon are linked to the reinforcement by a strong chemical reaction bond. However, carbide grains are also strongly linked to the matrix by mechanical bonds because they are embedded during the solidification in aluminium that has a higher coefficient of thermal expansion than aluminium carbide. Thus, Al_4C_3/C interfaces as well as Al/C interfaces are submitted to radial tension in opposition to the carbide–carbon reaction bonds.

As for silicon-reinforcement bonding, chemical diffusion bonds may exist because some silicon has diffused into the fibres during LMI. However, we think that such bonds are of little importance compared to the mechanical bonds that link silicon to fibre if consideration is given to resistance to debonding and to sliding. The coefficient of thermal expansion of silicon ($\approx 2.92\ 10^{-6}\ K^{-1}$) being low compared to the transverse coefficient of thermal expansion of the fibre, silicon grains are firmly fixed on the fibre by the interlocking effect promoted by the roughness. Such effects are efficient enough to grip together phases as different as porous alumina and pivalic acid and to resist shear stresses during sample cutting.[23] Moreover, silicon grains are submitted to compression stresses when they bridge fibres. Interlocking effects and compression stresses limit, even if they do not prevent, sliding at the silicon/fibre interface when silicon grains bridge fibres.

In silicon grains the gliding of Shockley partial dislocations in {111} planes which causes stacking faults more numerous in the narrowest part of the silicon bridges, releases some thermal stresses during quenching. Residual thermal stresses may, however, decrease the strength to failure of the fibre near these bridges.

The transverse stress to failure of the composites which results from these different bonds is weak as shown by the difficult thin film preparation (Section 2 and Fig. 1a). Because Al_4C_3/C or Si/C interfaces are rather rare, this low adhesion is not exclusive of stronger bonding at a few points at the interfaces.

4.3. Influence of the brittle phases on the mechanical behaviour

It is best first to discuss the influence of silicon grains because they are more numerous than aluminium carbide

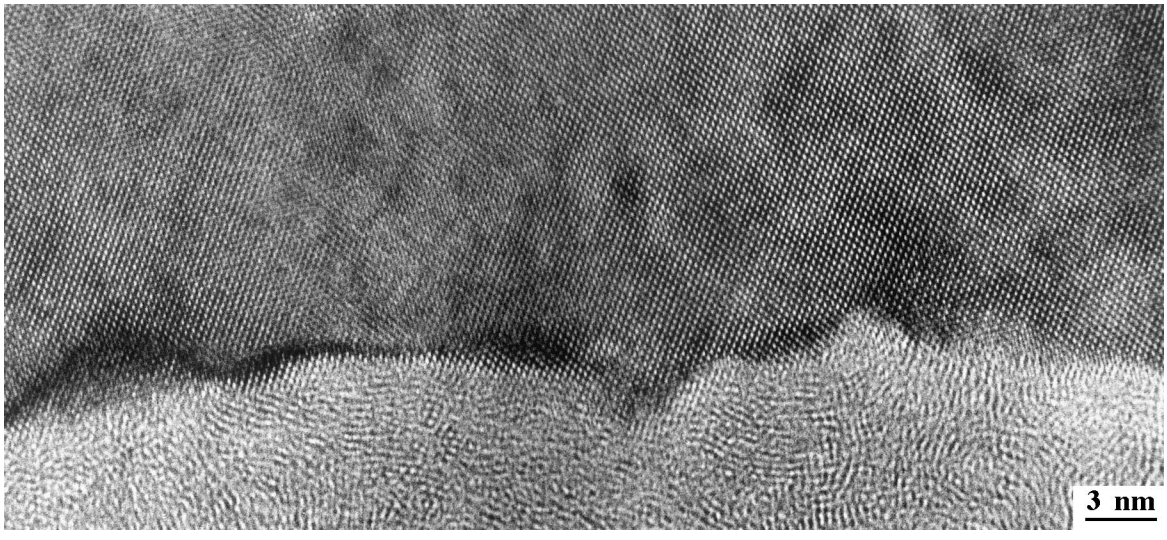

Fig. 8. Si/C. HRTEM images of the Si/fibre interface which shows that no Si–C reaction occurs during the composite fabrication.

grains and because they often bridge fibres. When fibres are bridged by a silicon grain, the composite has locally a brittle matrix. Because of the high volume fraction of fibres and because neighbouring fibres are generally in contact, it is reasonable to suppose that the Young modulus of the composites (Ec) is determined by the volume fraction of fibres ($Ec = 0.7$ Ef $= 263$ GPa). Silicon has the lowest Young modulus ($Esi = 163$ GPa) when compared to fibre and composite. During a tensile test, the composite strain is higher than that of a fibre submitted to the same stress and lower than that of silicon. The fibre/Si interface is thus submitted to shear stresses, the fibre being under greater tension than the silicon. These stresses are in opposite direction to the thermal stresses developed during cooling because of thermal mismatch.

It is not clear if silicon grains are more or less brittle than fibres. The tensile strength to failure found by Pearson et al. (2 GPa [24]) results in a strain to failure ($12.2\ 10^{-3}$) higher than that of fibres ($11.67\ 10^{-3}$). However, the strength to failure of brittle materials depends on flaw size. According to experimental results,[14] silicon grains seem to be more brittle than fibres and, thus, we analyse the impact of a silicon crack on the mechanical behaviour in this light.

It is helpful first to consider silicon grains linked to coated fibres in the M40J/Cp/A357 composite. Silicon grains have the critical size to initiate a fracture in the reinforcement[25] if no mechanism releases the stresses at the crack tip. When silicon is linked to the Cp, stresses will be released by decohesion either at the silicon/Cp interface or in the Cp (Section 4.1) depending on the debonding resistance as compared to the shear resistance of {0002} planes. After interface failure, a deformation of the outermost part of the coating under interfacial shear stresses can occur, despite radial compression stresses and surface roughness, because of its microporous microstructure and because fibres are under tension at the interface (see above). Microcracks and local shearing would release the stresses and may allow some sliding at the interface. These mechanisms delay the fibre and the composite failure. However, because these deformations are certainly limited and because the residual thermal stresses decrease the fibre strength, the composite breaks under a stress substantially lower than the value predicted by the law of mixtures (1300 instead of 3000 MPa) and with some pull out consistent with these model.

When a silicon grain bridges bare fibres, even if the resistance to debonding at the Si/fibre interface were low, sliding is restricted if not impossible at the interface without notching the fibre. Therefore, whatever the resistance to decohesion, stresses cannot be released at the crack tip and they will induce fibre failure. The simultaneous failure of silicon grains produces the simultaneous failure of many fibres and thus a brittle failure of the composite under low stress.

Owing to its well established deleterious effect, aluminium carbide is certainly more brittle than fibres. Moreover, despite their limited size, previous results[2–4] suggest that carbide grains can develop cracks which have the critical size to induce a fibre failure. When a crack notches the reinforcement, because of the turbostratic structure of the carbon and because of the axial tension at the Al_4C_3/C interface, it will be soon deflected in a direction parallel to the interface. In the case of coated fibres, the crack is deflected in the Cp. Sliding along the interfacial failure is possible despite the fibre roughness because of the limited width of the carbide grains (Section 3.2.2) and again because of the axial tension at the Al_4C_3/C interface. Thus, a carbide failure does not induce a fibre failure and the carbide grains have no influence on the strength of the M40J/Cp/A357 composite. In the case of a bare fibre, the notch will initiate a fibre failure when the tensile stress is high enough (Section 4.1). Aluminium carbide grains contribute to the weakness and brittleness of the M40J/A357 composite, but, due their low amount as compared to silicon grains, do not provide the main influence on M40J/A357 strength.

5. Conclusion

The main conclusions are as follows:

- the microstructure of the high modulus PAN based M40J carbon fibre is fully characterised; it is in better agreement with the microstructure of a high strength than of a high modulus PAN based carbon fibre,
- the pyrolytic carbon coating (Cp) used in the M40J/Cp/A357 composite consists of two layers of distinct microstructure, a layered structure near the fibre and a microporous structure near the matrix,
- the reaction of aluminium with carbon is limited during fabrication processing, particularly with the Cp; no reaction occurs between silicon and Cp or fibre,
- brittle phases, silicon and to a lesser extent aluminium carbide, are in contact with or bridge the fibres,
- the response of the composites to tensile stress parallel to the fibre axis is well described by the model of a brittle matrix reinforced by brittle fibres: the most important parameter is the high resistance to sliding due to interlocking effects between silicon grains and fibres and compression stresses in silicon bridges; it leads to a brittle and weak M40J/A357 composite but its influence is counterbalanced by the special structure of the Cp interphase in the M40J/Cp/A357 composite.

Acknowledgements

The authors wish to express their gratitude to Dr. M. Rabinovitch, Dr. M.H. Vidal-Sétif and ONERA-Chatillon for providing the samples and to Dr. M.H.V. and R. Valle for helpful discussions.

References

1. Renjie, W., *Proceedings of the International Conference on Composites Interfaces, Cleveland, OH*, ed H. Ishida. Elsevier, New York, 1988, pp. 43–56.
2. Chen, X. Q. and Hu, G. X. *Interfaces in Polymer, Ceramic and Metal Matrix Composites*, ed H. Ishida, Elsevier, New York 1988, pp. 381–388.
3. Qiong L., Gou, D. Z., Blucher, J. T. and Cornie, J. A. *Proceedings of the International Conference on Composites Interfaces (ICCI-III), Cleveland, OH*, ed. H. Ishida, Elsevier, New York, 1990, pp. 130–145.
4. Scott, V. D., Trumper, R. L. and Yang, M., *Composites Science and Technology*, 1991, **42**, 251–273.
5. Carpenter, J. C. and Lo, S. H. J., *J. Mat. Sci.*, 1992, **27**, 1827–1841 .
6. Diwanji, A. P. and Hall, I. W., *J. Mat. Sci.*, 1992, **27**, 2093–2100.
7. Perez, O., Patriarche, G., Lancin, M. and Vidal-Setif, M. H., *J. Phys. Coll C7, Suppl. J. Phys. III*, 1993, **3**, 1693–1698.
8. De Sanctis, M., Pelletier, S., Bienvehnu, Y. and Guigon, M., *Carbon*, 1994, **32**, 925–930.
9. Yang, H., Gu, M., Jiang, W. and Zhang, G., *J. Mat. Sci.*, 1996, **31**, 1903–1907.
10. Steffens, H. D., Reznik, B., Kruzhanov, V. and Dudzinski, W., *J. Mat. Sci.*, 1997, **32**, 5413–5417.
11. Hähnel, A., Pippel, E., Feldhoff, A., Schneider, R. and Woltersdorf, J., *J. Mat. Sci. Eng.*, 1997, **A237**, 173–179.
12. Rabinovitch, M., Vidal-Stif, M. H., Daux, J. C., Raviart, J. L., Gérard, J. L., Mevrel, R., Lancin, M. and Perez, O., *Proceedings of the 9th International Conference on Composite Materials (ICCM-9) Madrid*, ed. Miravete, Woodhead Pub. Cambridge UK, 1993, pp. 683–690.
13. Vidal-Sétif, M. H., Rabinovitch, M., Daux, J. C., Raviart, J. L., Laizet, J. C and Mevrel, R., *Proceedings of the 10th International Conference on Composites Materials (ICCM-10), Whistler BC, Canada*, ed A. Poursartip and K. Street, Woodhead Pub. Cambridge UK, 1995, pp. 449–456.
14. Vidal-Sétif, M. H., Lancin, M., Marhic, C., Valle, R., Raviart, J. L., Daux, J. C. and Rabinovitch, M., *Mat. Sci. Eng.,* in press.
15. Oberlin, A. In *Chemistry and Physics of Carbon, A Series Advance*, ed. P. A. Thrower, Marcel Dekker, New York, 1989, Vol. 22, pp. 1–143.
16. Peebles, L. H. Jr., *Int. Mat. Rev.*, 1994, **39**(2), 75–92.
17. Bourrat, X., Roche, E. J. and Lavin, J. G., *Carbon*, 1990, **28**, 435–446.
18. Knippenberg, W. F., *Philips Research Reports,* Philips research Laboratory, Eindhoven, Netherlands, 1963, Vol. 18, p. 199.
19. Guigon, M., Oberlin, A. and Desarmot, G., *Fibre Sci. Technol.*, 1984, **20**, 177–198.
20. Lamouroux, F., Bourrat, X., Naslain, R. and Sevely, J., *Carbon*, 1993, **31**(8), 1273–1288.
21. Feldhoff, A., Pippel, E. and Woltersdorf, J., *J. Microscopy*, 1997, **185**(2), 122–131.
22. Irwin, G. R., Fracture in Elastizität und Plastizität. In *Handbuch der Physik*, ed. S. Flügge. Springer, Berlin, 1958, pp. 551–5900.
23. Brissaud-Lancin, M., Riviere, A. and Philibert, J., *J. Phys. Chem. Solids*, 1982, **43**(2), 97–103.
24. Pearson, G. L., Read, W. T. Jr. and Feldmann, W. L., *Acta Metall.*, 1957, **5**, 181.
25. Ochiai, S., and Murakami, Y. *J. Mat. Sci.*, 1979, **14**, 831–840; Ochiai, S., Osamura, K., and Honjo, K., *Mat Sci. Eng. A*, 1992, **154**, 149–154